



OPEN

Indistinguishability of temporally separated pairwise two-photon state of thermal photons in Franson-type interferometry

Jiho Park, Heonoh Kim & Han Seb Moon✉

The phenomenon of Franson interference with time–energy entangled photon pairs beyond the single-photon coherence length observed upon nonlocal measurement at two space-like separated locations is of particular research interest. Herein, we determine the coherence length of temporally separated pairwise two-photon (TSPT) states of thermal photons emitted from a warm atomic ensemble in Franson-type interferometry, with the setup consisting of two spatially separated unbalanced Michelson interferometers beyond the coherence length of a thermal photon. Using a novel method of square-modulated thermal photons, we show that the sinusoidal Franson-type interference fringe of thermal photons is determined by the presence or absence of TSPT states (corresponding to the time delay between the long and short paths in Franson-type interferometry). We find that the indistinguishability of the TSPT state in the Franson-type interference is independent of the temporal separation of the thermal photons in the TSPT states.

A thorough understanding of the phenomenon of interference is essential to investigate the nature of light from the viewpoints of both classical and quantum physics. In this regard, the coherence of light is used to describe the correlation between the phases of two lights. In particular, interference can be observed as a function of the path-length difference in an interferometer within the coherence length of light. To suitably define the phase relation, a light should be separated and superposed. From the photon perspective, a single photon can only interfere with itself¹, and the observed interference pattern in this case can be described in terms of the quantum interference of the photon wavefunction. The coherence of photons is related to the intrinsic indistinguishability of particle trajectories that give rise to the interference pattern².

In this context, we consider Franson interference, which is a well-known second-order two-photon quantum interference phenomenon^{3,4}. In particular, the two-photon coherence length of a time–energy entangled photon pair beyond the single-photon coherence length is a counterintuitive phenomenon^{3–13}. To avoid single-photon interference in Franson interference, it is necessary that the path-length difference of the unbalanced interferometry setup is considerably longer than the coherence length of the one-photon state. Franson interference technique can determine the two-photon coherence length of an entangled photon pair⁶. The two-photon coherence length depends on the characteristics of the time–frequency entangled photon pair originating from various media^{4–13}.

Interestingly, the second-order interference (SOI) of thermal light in two independent unbalanced interferometers beyond the photon coherence length has been theoretically and experimentally reported^{14–18}. Although thermal photons are not energy–time entangled, this SOI beyond the coherence length in the Franson-type interferometry is a highly counterintuitive phenomenon^{14,16}.

In this work, we introduce the coherence length in a SOI with thermal photons as the indistinguishability of the temporally separated pairwise two-photon (TSPT) state in Franson-type interference for the first time. In this study, we propose the novel method for investigation of the temporal waveforms of thermal photons in Franson-type interferometry with and without the contribution of the TSPT states by using optical switching. We show that the SOI of the thermal photons in Franson-type interferometry is related to the intrinsic indistinguishability of the TSPT states of thermal photons, which is independent of the time delay between the temporally separated photons.

Department of Physics, Pusan National University, Geumjeong-Gu, Busan 46241, South Korea. ✉email: hsmoon@pusan.ac.kr

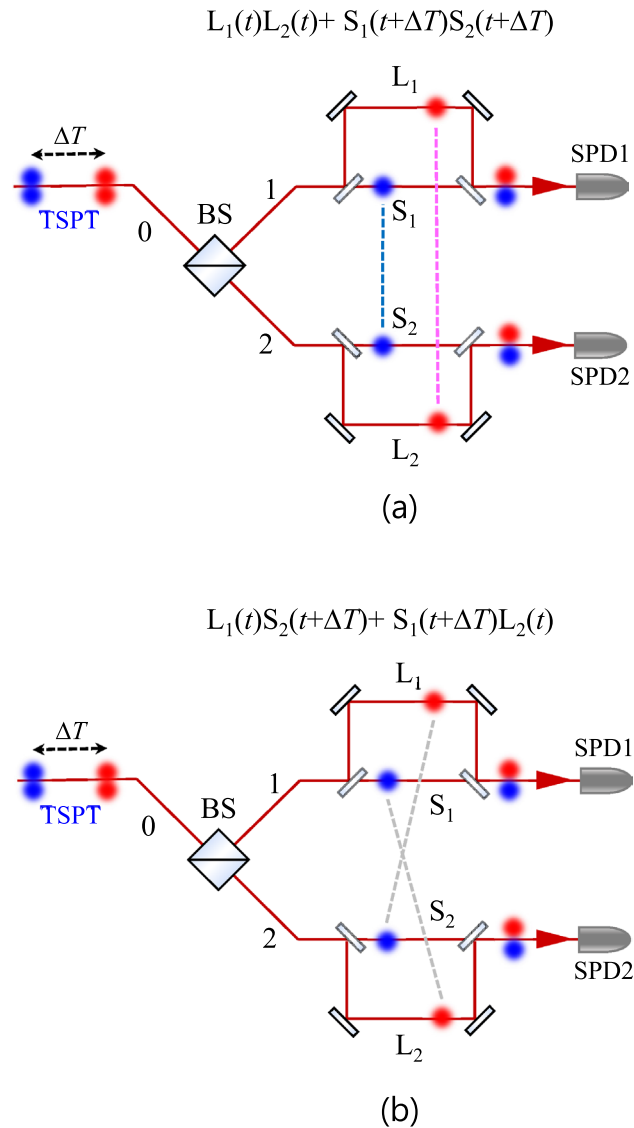


Figure 1. Indistinguishable events of temporally separated pairwise two-photon states in Franson-type interferometry. Coincidence events of the two detectors at $\tau=0$ in cases of (a) short-short (S_1S_2) and long-long (L_1L_2) paths and (b) long-short (L_1S_2) and short-long (S_1L_2) paths.

Indistinguishable events of temporally separated pairwise two-photon states

Here, we can define the coherence length of a two-photon state in a Franson-type interferometry as maximum path-length difference for possible interference. We first briefly describe the indistinguishable events of the CW-mode thermal light in Franson-type interferometry. The optical path-length difference between the long (L_i) and short (S_i) paths is considerably longer than the coherence length of the thermal light, and in the abovementioned notation, the subscripts represent the two spatial modes of the interferometer arms corresponding to the two output ports (1, 2) of the beam splitter (BS). The cases in Fig. 1a depict the phase-independent Hanbury Brown and Twiss (HBT) experiments corresponding to the second-order self-correlation function. Unlike the original Franson interference with entangled photon pairs, the indistinguishability of the two-photon state between the short-short (S_1S_2) and long-long (L_1L_2) paths in Fig. 1a affords no interference, because the two two-photon states of thermal photons are not correlated.

However, when we consider the time difference (ΔT) due to the path-length difference between the short and long paths, the two coincidentally detected photons of the long-short (L_1S_2) and short-long (S_1L_2) paths do not temporally overlap at the BS of the interferometer because the separation time can be considerably longer than the coherence time of the thermal light. However, the temporally separated thermal photons (red and blue circles) in the interferometer arms can be treated as a TSPT state (as indicated by the connecting gray dashed lines in Fig. 1b). The TSPT state with ΔT is described as¹⁹

$$|\Psi\rangle_{\text{TSPT}} = \frac{1}{\sqrt{2}} \left[a_1^\dagger a_2^\dagger(\Delta T) + a_2^\dagger a_1^\dagger(\Delta T) \right] |0, 0\rangle, \quad (1)$$

where a_i^\dagger denotes the photon creation operator, and the subscripts represent the two spatial modes of the interferometer arms according to the two output ports of the BS. The coincidence counts of the two detectors are related to the four cases of the S_1S_2 , L_1L_2 , L_1S_2 , and S_1L_2 paths, as shown in Fig. 1a,b.

However, the two photons in a TSPT state with ΔT can be coincidentally detected in the L_1S_2 and S_1L_2 paths, as shown in Fig. 1b. Although the TSPT states of the bunched photons are temporally separated beyond the coherence time of the CW-mode thermal light, the coincidence event of the TSPT state with ΔT via both the L_1S_2 and S_1L_2 paths is indistinguishable. The which-way information of the TSPT state of the thermal photons in the L_1S_2 and S_1L_2 paths of Franson-type interferometry is automatically erased. Furthermore, this interference is independent of the temporal separation of the TSPT state. Therefore, the coherence length of the TSPT state of the thermal photons in a Franson-type interferometry is unlimited.

The temporal waveform of the CW-mode bunched photons in Franson-type interferometry corresponds to the second-order correlation function $G^{(2)}(t_1, t_2)$ in the two unbalanced interferometers, which can be expressed as¹⁴

$$G^{(2)}(t_1, t_2) = G^{(1)}(t_1, t_1)G^{(1)}(t_2, t_2) + \eta \left| G^{(1)}(t_1, t_2) \right|^2. \quad (2)$$

here $G^{(1)}(t_1, t_2)$ represents the first-order correlation function of the thermal photons, where t_i ($i = 1$ and 2) denotes the relative arrival times of the photons at SPD1 and SPD2, respectively. In addition, η represents the thermal fraction coefficient, including the time uncertainties of the both SPDs and their electronic time jitter.

The second term $\left| G^{(1)}(t_1, t_2) \right|^2$ in Eq. (2) can be expressed as

$$\left| G^{(1)}(t_1, t_2) \right|^2 = \left\{ \begin{array}{l} \left| G^{(1)}(t_{L1}, t_{S2}) \right|^2 \\ + \left| G^{(1)}(t_{L1}, t_{L2}) + G^{(1)}(t_{S1}, t_{S2}) + G_{\text{TSPT}}^{(1)}(t_{L1}, t_{S2}) + G_{\text{TSPT}}^{(1)}(t_{S1}, t_{L2}) \right|^2 \\ + \left| G^{(1)}(t_{S1}, t_{L2}) \right|^2 \end{array} \right\}, \quad (3)$$

where t_i ($i = S_1, S_2, L_1,$ and L_2) denotes the relative arrival times of the photons at SPD1 and SPD2 via the short (S_1, S_2) and long (L_1, L_2) paths, respectively. In particular, $G_{\text{TSPT}}^{(1)}$ corresponds to the TSPT state with ΔT in the L_1S_2 and S_1L_2 paths. Moreover, $G_{\text{TSPT}}^{(1)}(t_{L1}, t_{S2})$ and $G_{\text{TSPT}}^{(1)}(t_{S1}, t_{L2})$ describe the effects of the TSPT states in Franson-type interferometry, as in the case shown in Fig. 1b.

Additionally, the time difference $\tau = t_1 - t_2$ between the detection times of both SPDs is determined by the path-length differences of the four possible scenarios concerning the short and long paths. The first-order correlation function $g^{(1)}(\tau)$ is applicable to the two cases of the S_1S_2 and L_1L_2 paths whereas $g_{\text{TSPT}}^{(1)}(\tau)$ corresponds to the TSPT state with ΔT in the cases of L_1S_2 and S_1L_2 . The thermal light in the Doppler-broadened atomic system can be expressed as $g^{(1)}(\tau) = g_{\text{TPST}}^{(1)}(\tau) = \exp[-\pi(\tau/\tau_c)^2]$, where τ_c denotes the coherence time of the thermal light. Therefore, the normalized second-order correlation function $g^{(2)}(\tau)$ in Franson-type interferometry can be described as

$$g^{(2)}(\tau) = 1 + \frac{\eta}{4} \left\{ \begin{array}{l} \left| g^{(1)}(\tau - \Delta T) \right|^2 \\ + 2 \left| g^{(1)}(\tau) \right|^2 + (e^{i(\phi_L - \phi_S)} + e^{-i(\phi_L - \phi_S)}) \left| g_{\text{TPST}}^{(1)}(\tau) \right|^2 \\ + \left| g^{(1)}(\tau + \Delta T) \right|^2 \end{array} \right\}, \quad (4)$$

where the phase factors ϕ_L and ϕ_S can be expressed as $\phi_L = \frac{\omega}{c}(L_1 - L_2)$ and $\phi_S = \frac{\omega}{c}(S_1 - S_2)$, respectively. Here, ω and c denote the angular frequency of the signal photon and the speed of light in vacuum, respectively. In the case of time-energy entangled photon pairs, the second-order correlation function of the photon pair is proportional to the temporal two-photon waveform shapes in the Franson interferometer⁷. Therefore, $g^{(2)}(\tau)$ in Eq. (4) represents the temporal waveform of the thermal light in Franson-type interferometry (see Supplementary Note 1 for further details²⁰).

While the original Franson interference is related to the second-order cross-correlation function with entangled photon pairs, the term for SOI in this experiment is related to the second-order self-correlation function of the TSPT state of the thermal light. In particular, the observed interference is contributed to the temporally separated thermal photons, with the separation corresponding to the time difference of the long-short (L_1S_1 and L_2S_2) paths of both the unbalanced interferometers.

The thermal light used in our experiment was obtained from a Doppler-broadened cascade-type atomic ensemble based on the $5S_{1/2} - 5P_{3/2} - 5D_{5/2}$ transition of ^{87}Rb ²¹. The properties of our real thermal light from the warm Rb atoms are not only bright but also long-coherence length. As shown in Fig. 2, the Franson-type interferometry setup consists of two unbalanced Michelson interferometers (UMIs) with a large path difference. The long paths (L_1 and L_2) of both UMIs are 2-m long, including an optical fiber mirror.

To confirm the role of the TSPT state of thermal photons in Franson-type interferometry, we modulated the CW-mode thermal photons to a square form with an electro-optic modulator (EOM), as shown in Fig. 2. With this setup, we can determine whether the TSPT state is present or absent by adjusting the modulation period of the EOM. In particular, when the period of the modulation input signal is double the ΔT value, the TSPT state in Fig. 1b is absent. In this experimental scenario, we consider the observation of the SOI fringe with thermal photons as a function of path-length differences Δx_1 or Δx_2 of the short arms of both UMIs.

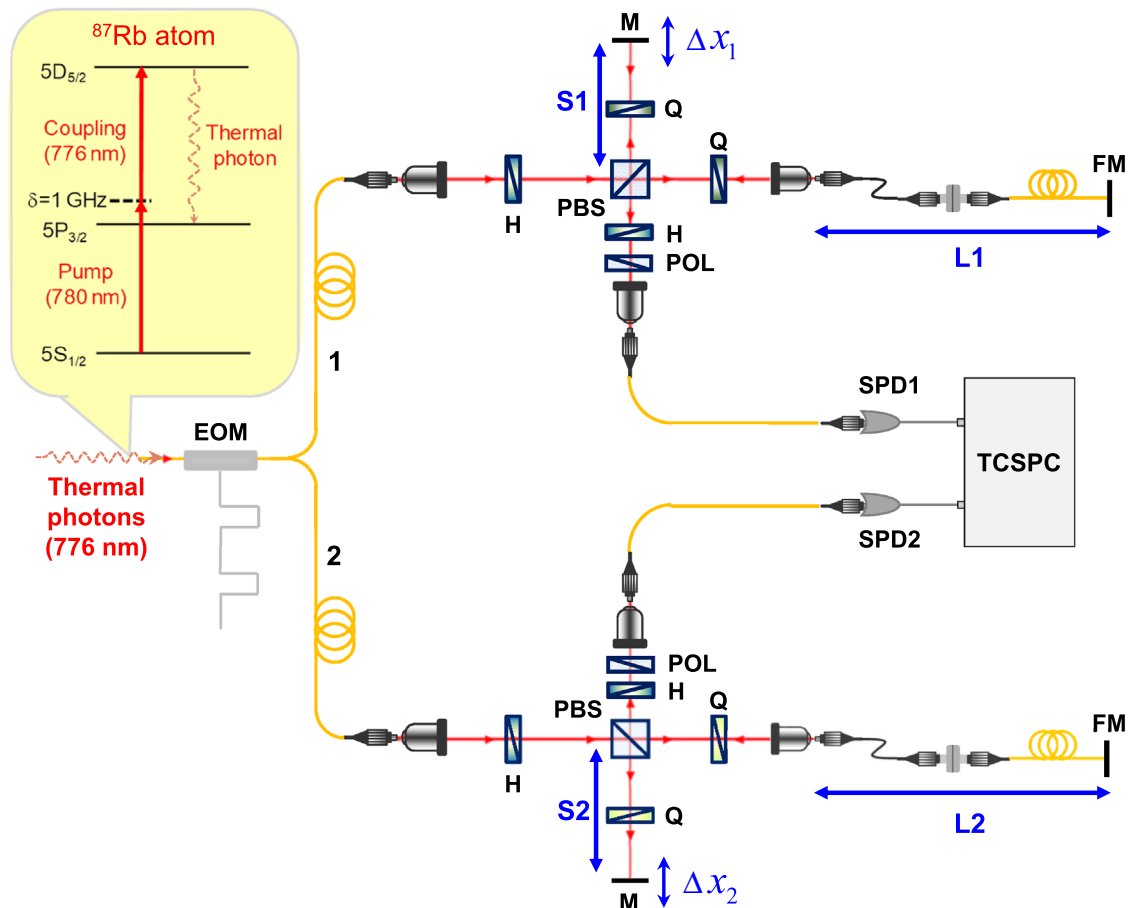


Figure 2. Experimental setup for Franson-type interference with thermal light. SOI obtained using unbalanced Michelson interferometers with large path difference (EOM: electro-optic modulator; H: half-wave plate; Q: quarter-wave plate; M: mirror; POL: polarizer; PBS: polarizing beam splitter; FM: fiber mirror; SPD: single-photon detector; TCSPC: time-correlated single-photon counting module). Numerically calculated phase-matching function values as a function of the propagating angle (θ) of the generated FWM for various tilt angles (θ_d) of the driving laser in the four-wave mixing process using a Doppler-broadened cascade-type atomic system.

Experimental results and discussion

First, we consider the TSPT state ($|\Psi\rangle_{\text{TSPT}}$) with ΔT mentioned in Eq. (1) (as shown in the experimental schematic of Fig. 3a), when the period of the square modulation corresponds to $\Delta T = 20$ ns. To understand the characteristics of the square-modulated thermal photons in the Franson-type interferometry, we measured the second-order self-correlation functions of the square-modulated thermal photons in the four cases of the S_1S_2 , L_1L_2 , L_1S_2 , and S_1L_2 paths by blocking the optical paths of both UMIs in Fig. 2; the results are shown in Fig. 3b. These results correspond to those of the phase-independent HBT experiment. Here, the triangular form of the coincidence background is due to the convolution of the input square modulation of thermal photons, and its period corresponds to that of the square modulation.

In the cases of S_1S_2 and L_1L_2 (corresponding to the red dashed lines in Fig. 3a), the coincidence count at $\tau = 0$ is maximum and $g^{(2)}(0)$ is estimated to be 1.76(2), which corresponds to the bunched-light $g^{(2)}(0)$ value of the CW-mode thermal photons (see Supplementary Note 2 for further details²⁰). In addition, in the cases of S_1L_2 and L_1S_2 , we note that $g^{(2)}(\Delta T)$ and $g^{(2)}(-\Delta T)$ exhibit their maximum values at the time delay between the short and long paths. In particular, both photons separated by ΔT before the BS can be coincidentally detected at $\tau = 0$ in the cases of L_1S_2 or S_1L_2 (blue dashed lines in Fig. 3a); however, we note that there is no correlation between the two temporally separated photons (Fig. 3b). Because of the breaking of the optical paths in the Franson-type interferometer, the which-way information of both photons is determined, and we cannot consider the TSPT state with ΔT in the results shown in Fig. 3b.

Next, we consider the four cases in Fig. 3 simultaneously in the Franson-type interferometry. Here, it is obvious to assume that the temporal waveform in the Franson-type interferometry is the sum of the four results shown in Fig. 3b. However, interestingly, we observe the interference effect from the temporal waveforms of thermal photons in the Franson-type interferometry, as shown in Fig. 4a, b, under constructive and destructive interference conditions, respectively. Under the constructive interference condition (Fig. 4a), we note that

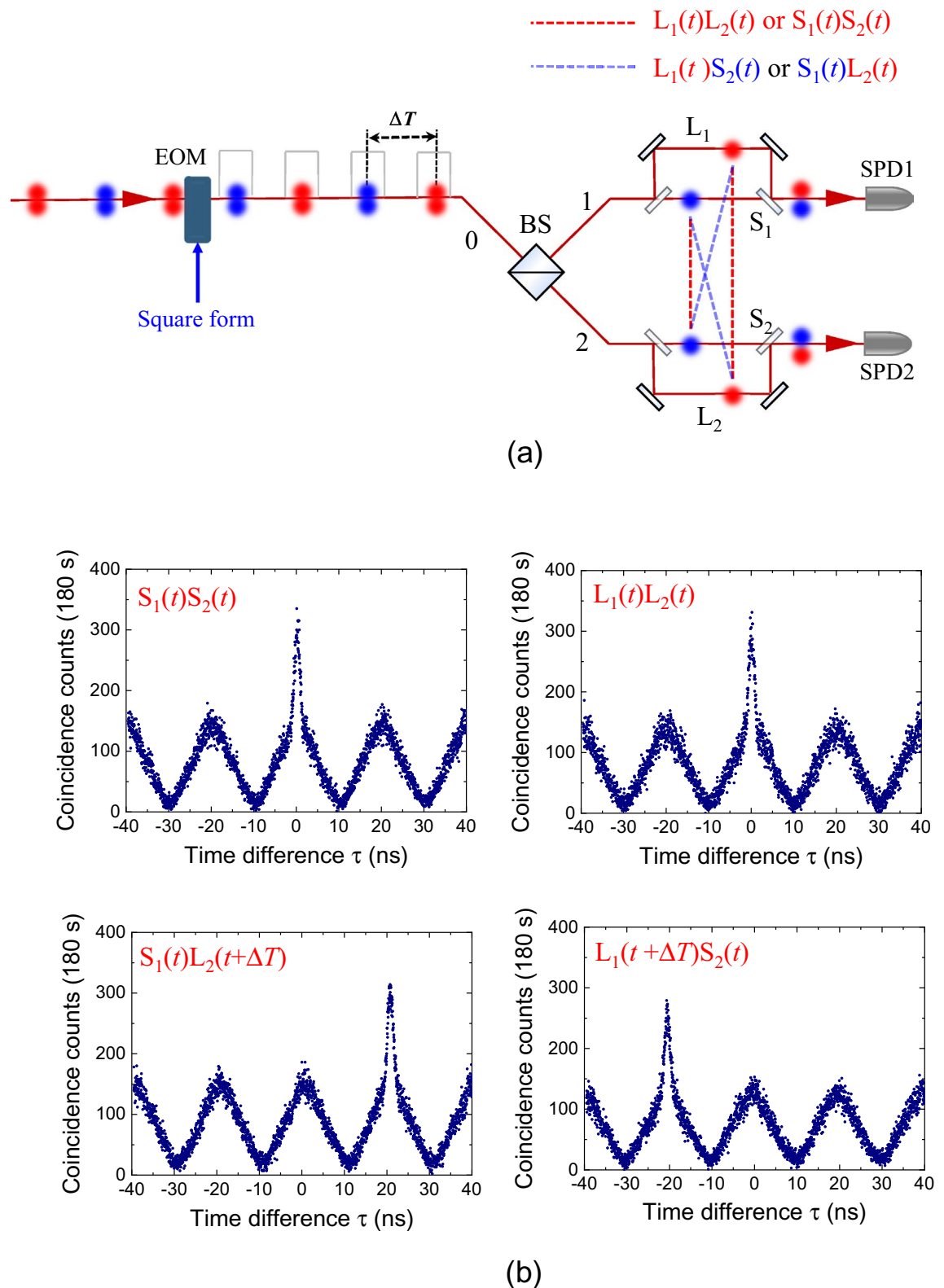


Figure 3. Square-modulated thermal photons with period of ΔT . (a) Experimental schematic for measurement of the second-order self-correlation functions of the square-modulated thermal photons with period of 20 ns. (b) Coincidence events in four cases of short-short (S_1S_2), long-long (L_1L_2), long-short (L_1S_2), and short-long (S_1L_2) paths.

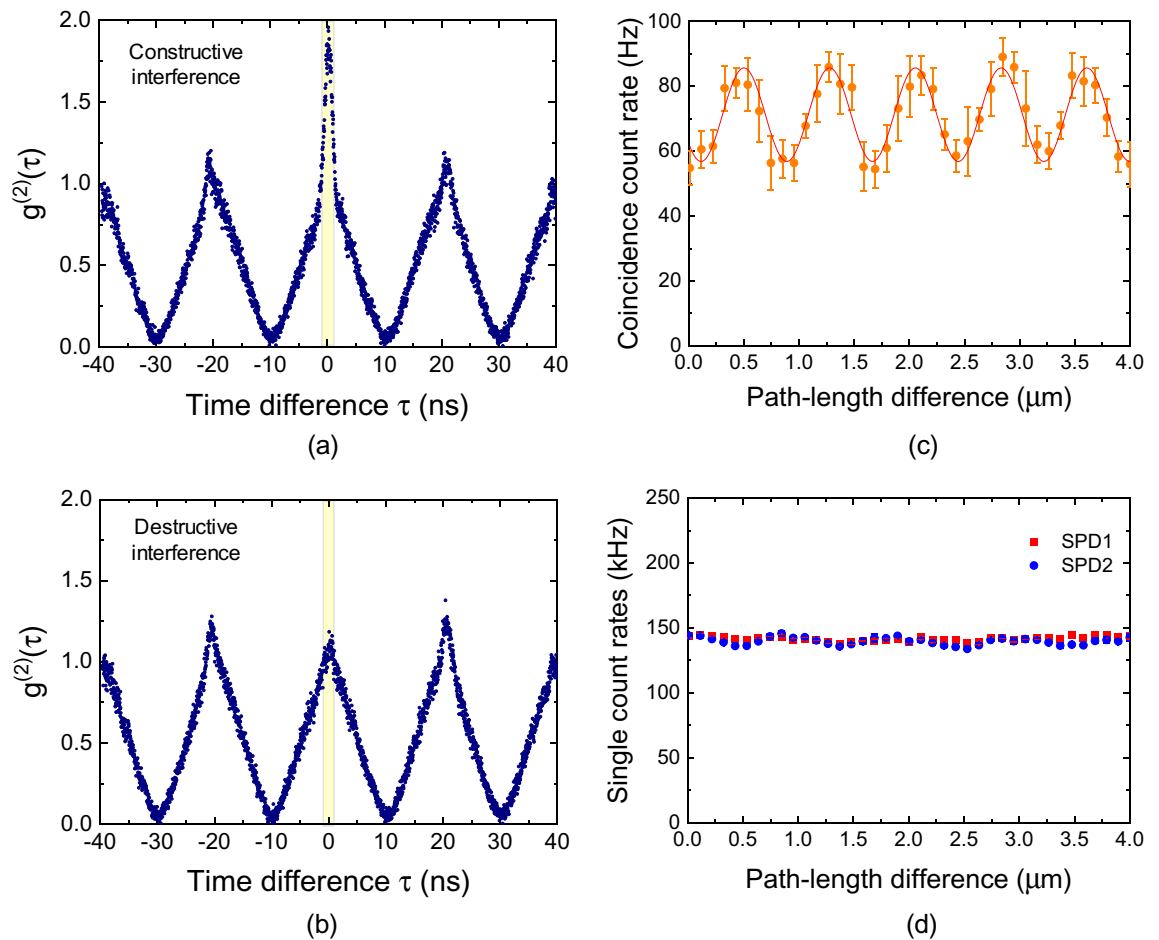


Figure 4. Temporal waveforms of thermal light obtained with Franson-type interferometer. Experimental (blue dots) and theoretical (red curves) results for (a) the constructive SOI condition of $\phi_L - \phi_S = 0$, (b) destructive SOI condition of $\phi_L - \phi_S = \pi$. (c) SOI fringe of the thermal light as a function of the path-length difference between both unbalanced Michelson interferometers (Δx_1 changed and fixed at $\Delta x_2 = 0$). (d) Single count rates of SPD1 (blue circles) and SPD2 (red circles) as a function of the path-length difference.

the temporal waveforms of thermal light consist of two side peaks due to the long-short (L_1S_2 and L_2S_1) path mismatch of the UMIs and the central peak at $\tau = 0$. Importantly, the central peak for constructive interference in Fig. 4a is not the sum of the self-correlation results shown in Fig. 3b. The magnitude of the central peak is four times that of both side peaks. Next, when Δx_1 of the short arm of the UMI (Fig. 2) is varied, we observe the magnitude variation of the central peak. In Fig. 4b, the value of $g^{(2)}(0)$ at $\tau = 0$ is close to the normalized value of 1, corresponding to destructive interference. Therefore, to understand this phase-sensitive interference of second-order self-correlation in the Franson-type interferometry, we should consider the indistinguishable events of the TSPT state with ΔT , as shown in Fig. 3a.

The $g^{(2)}(0)$ term in Eq. (4) can be simply expressed as

$$g^{(2)}(0) = 1 + \frac{\eta}{2} \left[1 + \cos \left(\frac{\omega_0}{c} (L_1 - L_2) - \frac{\omega_0}{c} (S_1 - S_2) \right) \right]. \quad (5)$$

Sinusoidal SOI fringes can be obtained according to the path-length difference between the long (L_1, L_2) and short (S_1, S_2) arms of both UMIs.

When we measure the coincidence counting of the SPD1 and SPD2 with a 2.5-ns temporal window (corresponding to the yellow box shown in Fig. 4a,b), we can observe the sinusoidal SOI fringe of the thermal photon, as shown in Fig. 4c. In our experiment, we varied Δx_1 or Δx_2 of the short arms by using the translator stages to investigate the SOI fringe variation as a function of the path-length difference of both UMIs.

Here, the visibility of sinusoidal SOI fringe in Fig. 4c is estimated to be 22%. We note that the visibility of the SOI fringe of thermal photon is limited by the time jitter of the employed SPDs and the temporal window for coincidence counting (see Supplementary Note 3 for further details²⁰). The maximum and minimum values of the sinusoidal SOI fringe in Fig. 4c correspond to the temporal waveforms of the thermal light in Fig. 4a,b, respectively. Simultaneously, we analyzed the single count rates of the SPD1 and SPD2, as shown in Fig. 4d. We

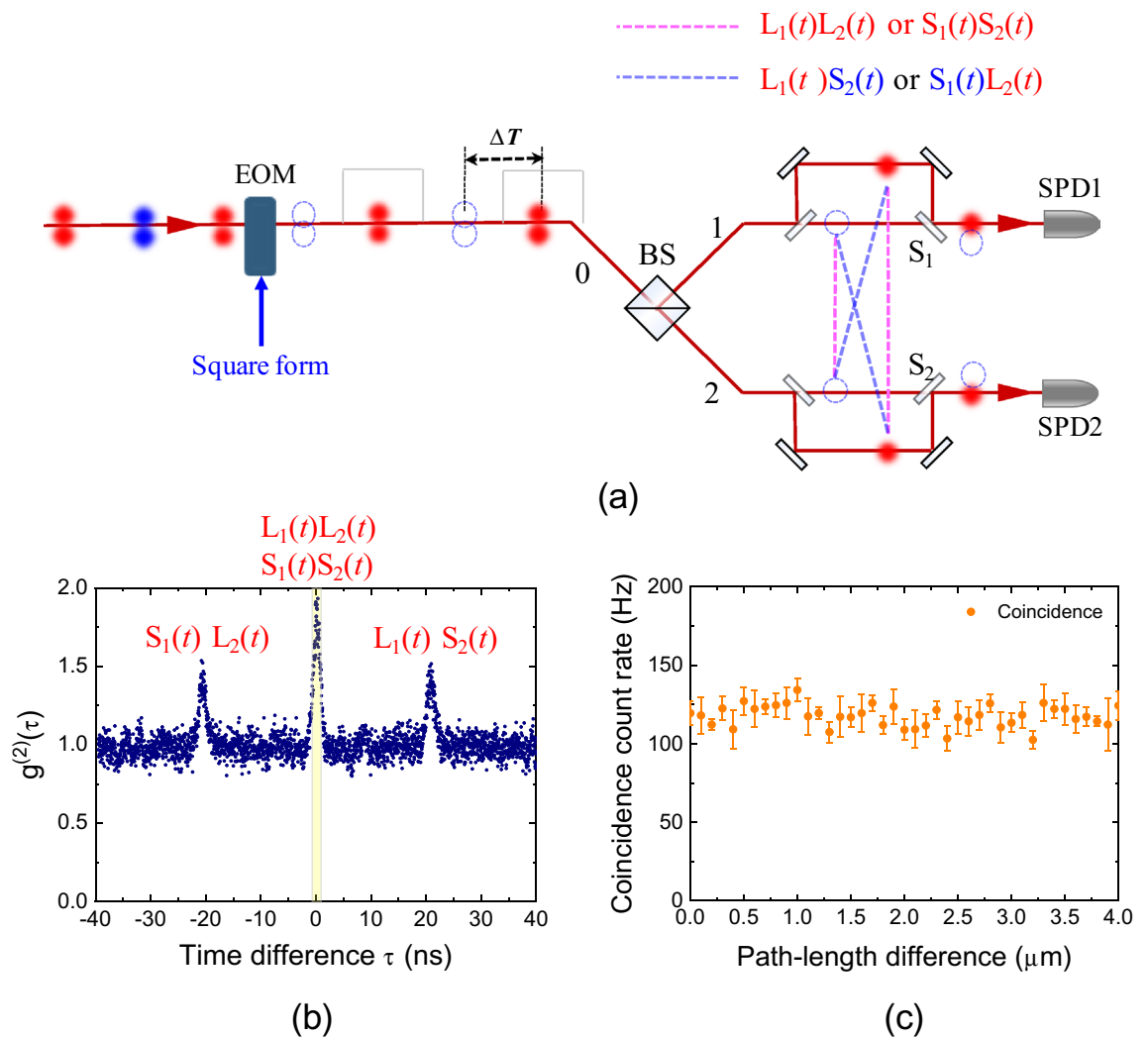


Figure 5. Absence of TSPT state with ΔT in Franson-type interferometry. (a) Possible coincidence events of both SPDs at $\tau=0$ with the switching off of the photons (blue circles) after ΔT from the instant of switching on of the photons (red circles). (b) Temporal waveform of thermal photons in Franson-type interferometer without the TSPT state with ΔT . (c) Coincidence count rate as a function of the path-length difference (Δx_1 or Δx_2).

cannot see the sinusoidal interference fringe as a function of the path-length difference of UMIs because the long-short path-length difference of UMI is 10 times longer than the 0.5-m coherence length of thermal photon.

Next, we “lift” or “break” the TSPT state with ΔT using optical switching with the EOM. When the period of the square modulation is set to $2\Delta T=40$ ns, we can switch off the photons (blue circles) after ΔT from the instant of the switching on of the photons (red circles), as shown in Fig. 5a. In this experimental scenario, we cannot consider $|\Psi\rangle_{\text{TSPT}}$ with ΔT expressed in Eq. (1). In this case, the $|g_{\text{TSPT}}^{(1)}(\tau)|^2$ term in Eq. (4) is absent. The $g^{(2)}(\tau)$ term in Franson-type interferometry is independent of the phase difference, as can be inferred from Fig. 5b. In our study, the $g^{(2)}(0)$ value was estimated to be 1.75(2), corresponding to that for the constructive interference in Fig. 4a. We note here that the magnitude of the central peak is twice that of both side peaks. Unlike the temporal waveforms shown in Fig. 4a,b, the square modulation of the thermal photons, corresponding to the background in Fig. 5b, does not afford a triangular shape. This is because the triangular form of the coincidence background is out of phase among the second-order self-correlation functions of the square-modulated thermal photons in the four cases (S_1S_2 , L_1L_2 , L_1S_2 , and S_1L_2) (see Supplementary Note 4 for further details²⁰).

When the detection time difference τ is equal to zero, Eq. (5) can be expressed as $g^{(2)}(0) = 1 + \frac{\eta}{2}$ for the two cases of short-short (S_1S_2) and long-long (L_1L_2) paths, where the thermal fraction coefficient η is estimated to be 0.75. In Fig. 5c, we cannot observe any sinusoidal SOI fringes as a function of the path-length difference. Therefore, the SOI of thermal photons in Franson-type interferometry is related to the intrinsic indistinguishability of the TSPT states of thermal photons, which is independent of the time delay between the temporally separated photons.

Conclusion

In conclusion, we have determined the coherence length of TSPT states of thermal photons emitted from a warm atomic ensemble in Franson-type interferometry. Using the novel method of square-modulated thermal photons, we could actively choose whether or not to erase which-path information of the TSPT states of thermal photons in Franson-type interferometry. We confirmed that the cause of SOI of thermal photons in Franson-type interferometry is the intrinsic indistinguishability of the TSPT states of thermal photons. Because the indistinguishability of the TSPT state in the Franson-type interference is independent of the temporal separation of the thermal photons in the TSPT states, the coherence length of the TSPT state of the thermal photons in a Franson-type interferometry is unlimited.

Received: 26 November 2021; Accepted: 17 March 2022

Published online: 31 March 2022

References

1. Dirac, P. A. M. *The Principles of Quantum Mechanics* 4th edn. (Oxford University, USA, 1958).
2. Mandel, L. Coherence and indistinguishability. *Opt. Lett.* **16**, 1882–1883 (1991).
3. Franson, J. D. Bell inequality for position and time. *Phys. Rev. Lett.* **62**, 2205 (1989).
4. Ou, Z. Y., Zou, X. Y., Wang, L. J. & Mandel, L. Observation of nonlocal interference in separated photon channels. *Phys. Rev. Lett.* **65**, 321 (1990).
5. Brendel, J., Mohler, E. & Martienssen, W. Time-resolved dual-beam two-photon interferences with high visibility. *Phys. Rev. Lett.* **66**, 1142 (1991).
6. Park, J., Jeong, T., Kim, H. & Moon, H. S. Time-energy entangled photon pairs from Doppler-broadened atomic ensemble via collective two-photon coherence. *Phys. Rev. Lett.* **121**, 263601 (2018).
7. Park, J., Kim, D., Kim, H. & Moon, H. S. High-visibility Franson interference of time-energy entangled photon pairs from warm atomic ensemble. *Opt. Lett.* **44**(15), 3681–3684 (2019).
8. Honjo, T., Takesue, H. & Inoue, K. Generation of energy-time entangled photon pairs in 1.5- μm band with periodically poled lithium niobate waveguide. *Opt. Express* **15**(4), 1679–1683 (2007).
9. Sarrafi, P. *et al.* High-visibility two-photon interference of frequency-time entangled photons generated in a quasi-phase-matched AlGaAs waveguide. *Opt. Lett.* **39**(17), 5188–5191 (2014).
10. Jayakumar, H. *et al.* Time-bin entangled photons from a quantum dot. *Nat. Commun.* **5**, 4251 (2014).
11. Peiris, M., Konthasinghe, K. & Muller, A. Franson interference generated by a two-level system. *Phys. Rev. Lett.* **118**, 030501 (2017).
12. Grassani, D. *et al.* Micrometer-scale integrated silicon source of time-energy entangled photons. *Optica* **2**, 88–94 (2015).
13. Rogers, S., Mulkey, D., Lu, X., Jiang, W. C. & Lin, Q. High visibility time-energy entangled photons from a silicon nanophotonic chip. *ACS Photon.* **3**, 1754 (2016).
14. Tamma, V. & Seiler, J. Multipath correlation interference and controlled-not gate simulation with a thermal source. *New J. Phys.* **18**, 032002 (2016).
15. Tamma, V. The physics of thermal light second-order interference beyond coherence. *Phys. Scr.* **93**, 124010 (2018).
16. Ihn, Y. S., Kim, Y., Tamma, V. & Kim, Y.-H. Second-order temporal interference with thermal light: interference beyond the coherence time. *Phys. Rev. Lett.* **119**, 263603 (2017).
17. Park, J., Kim, H. & Moon, H. S. Second-order interference of true thermal light from a warm atomic ensemble in two independent unbalanced interferometers. *Photon. Res.* **9**, 49–53 (2021).
18. Lee, G.-H., Im, D.-G., Kim, Y., Kim, U.-S. & Kim, Y.-H. Observation of second-order interference beyond the coherence time with true thermal photons. *Opt. Lett.* **45**(24), 6748–6751 (2021).
19. Kim, D., Park, J., Jeong, T., Kim, H. & Moon, H. S. Two-photon interference between continuous-wave coherent photons temporally separated by a day. *Photon. Res.* **8**, 338–342 (2020).
20. See the Supplementary Material for detailed descriptions of the temporal waveforms of CW-mode thermal light in Franson-type interferometer, the limitation of maximum $g^{(2)}(0)$ value of thermal light from Doppler-broadened warm atomic vapor, the maximum visibility of sinusoidal two-photon interference with thermal photon considering coincidence window, and the second-order self-correlation function of square-modulated thermal photons with period of $2\Delta T$.
21. Park, J., Jeong, T. & Moon, H. S. Temporal intensity correlation of bunched light from a warm atomic vapor with a ladder-type two-photon transition. *Sci. Rep.* **8**, 10981 (2018).

Acknowledgements

This work was supported by the National Research Foundation of Korea (NRF) (Nos. 2021R1A2B5B03002377 and 2020M3E4A1080030) and the Ministry of Science and ICT (MSIT), Korea, under the Information Technology Research Center (ITRC) support program (IITP-2021-2020-0-01606) supervised by the Institute of Information and Communications Technology Planning and Evaluation (IITP).

Author contributions

H.S.M. conceived the project. J.P., H.K., and H.S.M. designed the experimental setup and performed the experiments. J.P., H.K., and H.S.M. discussed the results and contributed to the writing of the manuscript.

Competing interests

The authors declare no competing interests.

Additional information

Supplementary Information The online version contains supplementary material available at <https://doi.org/10.1038/s41598-022-09516-y>.

Correspondence and requests for materials should be addressed to H.S.M.

Reprints and permissions information is available at www.nature.com/reprints.

Publisher's note Springer Nature remains neutral with regard to jurisdictional claims in published maps and institutional affiliations.



Open Access This article is licensed under a Creative Commons Attribution 4.0 International License, which permits use, sharing, adaptation, distribution and reproduction in any medium or format, as long as you give appropriate credit to the original author(s) and the source, provide a link to the Creative Commons licence, and indicate if changes were made. The images or other third party material in this article are included in the article's Creative Commons licence, unless indicated otherwise in a credit line to the material. If material is not included in the article's Creative Commons licence and your intended use is not permitted by statutory regulation or exceeds the permitted use, you will need to obtain permission directly from the copyright holder. To view a copy of this licence, visit <http://creativecommons.org/licenses/by/4.0/>.

© The Author(s) 2022